文章编号:1006-9941(2020)08-0749-10

Numerical Estimation of Crack Depth in Curved Surfaces of Polymer Bonded Explosives Using Rayleigh Surface Wave

JIANG Chang[1,2], **YANG Zhan-feng**[1], **LI Wei-bin**[2], **ZHANG Wei-bin**[1], **TIAN Yong**[1]

(1. *Institute of Chemical Materials, China Academy of Engineering Physics, Mianyang* 621999, *China*; 2. *School of Aerospace Engineering, Xiamen University, Xiamen* 361005, *China*)

Abstract: Cracks in polymer bonded explosives (PBXs) may occur during manufacturing, transportation and storage stages. The surface crack of explosives has an important influence on their mechanical properties and detonation performance. Quantitative detection of the depth of the surface crack is of great significance to the process of surface crack removal. The numerical simulation of surface crack depth estimation was investigated by using Rayleigh surface waves which propagate along the cylindrical and spherical surfaces of PBXs. The propagation patterns of surface waves were studied on these two types of surfaces. The reflection and transmission of surface waves at different frequencies in PBXs with crack of varied depth were simulated through the finite element method (FEM).The FEM results indicate that the depth of crack in curved surfaces can be deduced according to the amplitude variations of reflected and transmitted waves.

Key words: Rayleigh wave; curved surface; polymer bonded explosive; crack depth; simulation

CLC number: TJ55; O429; O343 **Document code**: A **DOI**: 10.11943/CJEM2019156

1 Introduction

Polymer bonded explosives (PBX), as an important type of national defense and military product, possesses the advantages of high energy density, great mechanical properties and superior security. However, cracks often occur in the process of forming, machining and post-processing, leading to performance degradations of the explosives[1-5].Ultrasonic inspection is an important nondestructive technique for assessment of many types of macro and micro defects in contrast to the industrial computed tomography[6-8]. Given that cracks usually initiate from the surface, ultrasonic surface wave seems to be relatively more feasible and appropriate for the evaluation of crack depth in PBXs providing more sensitivity than others with most of the wave energy confined in the vicinity of the free surface within a depth of the specimen under test[9].

Researches have been reported on ultrasonic crack detection in plates, but references to crack depth determination with respect to curved surfaces of PBXs are still limited for the moment[10]. In a recent investigation, C. He[11] presented a quantitative characterization method for estimating surface crack depth employing electromagnetic acoustic transducers. Other studies have also demonstrated considerable results on the interaction of Rayleigh waves and cracks[12]. However, the above studies investigate cracks only on the planar surface, while distinctive propagation patterns of surface waves are supposed to turn up concerning curved surfaces. To date, few

Received Date: 2019-06-03; **Revised Date**: 2019-09-27

Published Online: 2020-03-12

Project Supported: National Natural Science Foundation of China (No. 11572294)

Biography: JIANG Chang (1995-), male, postgraduate. Research field: Ultrasonic testing. e-mail: jcxmu@qq.com

Corresponding author: YANG Zhan-feng (1977-), male, research associate. Research field: Ultrasonic testing of PBXs.
e-mail: yangzf@caep.cn

LI Wei-bin (1982-), male, associate professor. Research field: Ultrasonic testing. e-mail: lwbwave@163.com

引用本文:江畅,杨占锋,李卫彬,等. 基于瑞利表面波的曲面PBX表面裂纹深度检测的数值模拟[J]. 含能材料,2020,28(8):749-758.
JIANG Chang, YANG Zhan-feng, LI Wei-bin, et al. Numerical Estimation of Crack Depth in Curved Surfaces of Polymer Bonded Explosives Using Rayleigh Surface Wave[J]. *Chinese Journal of Energetic Materials (Hanneng Cailiao)*, 2020, 28(8):749-758.

works on crack detection on curved surfaces using surface waves can be found.

This paper aims to provide solutions of ultrasonic method for quantitatively estimating crack depth on cylindrical and spherical surfaces of PBXs. An inversion method for crack depth estimation involving a benchmark of the transmission and reflection curves is proposed. By means of the finite element method (FEM), wave motion of surface wave on cylindrical and spherical PBXs are studied, along with the reflection and transmission waves resulted from the interaction of Rayleigh waves and cracks of different depths. Results are analyzed considering the theoretical predictions. Comparison of the simulation results with certain references is made to ensure the credit of this numerical study.

2 Theory

2.1 Rayleigh surface wave

Rayleigh waves are a type of surface wave which propagate near the surface of solids and decrease exponentially in amplitude as distance from the surface increases. Many researches have studied the wave velocity of Rayleigh surface wave regarding different characteristics of materials [13]. The major axis of the elliptic orbits is vertical to the surface, and the in-plane motion of a particle is retrograde at shallow depths and prograde at greater depths. The earliest approximate expression was given by $c_R = (0.87 + 1.12\nu)/(1+\nu) \cdot c_2$, where c_2 is the shear wave velocity.

2.2 Dispersion in curved surfaces

The Rayleigh wave dispersion is usually observed when the properties of the materials alter with depth such as propagations in the earth and multi-layered structures. On the other hand, the influence of curvature radii on the wave number and wave velocity has been theoretically analyzed. The Rayleigh wave velocity in curved surface is given by[13]

$$c = c_R\left(1 - \frac{1}{2}\frac{c_R}{\omega C}\left(\frac{A}{\rho_\alpha} + \frac{B}{\rho_\beta}\right)\right) \tag{1}$$

where c_R denotes the Rayleigh wave velocity along a plane surface, ω is the angular frequency, ρ_α and ρ_β are the curvature radii parallel and perpendicular to the propagation direction, respectively. A, B and C are expressed as follows

$$\begin{aligned} A &= (\lambda + 2\mu)\left(2\sqrt{1-a} - a - a\sqrt{1-b}\right) \\ B &= -2\mu\left(\frac{a\sqrt{1-b}}{1-a} + \frac{\sqrt{1-a}}{1-b}\right) \\ C &= 2[(\lambda + 2\mu)a] - \mu(5 - 2b) \\ a &= \frac{c_R^2}{c_1^2},\ b = \frac{c_R^2}{c_2^2} \end{aligned} \tag{2}$$

where c_1 and c_2 are the longitudinal and transverse wave velocities, respectively, and λ,μ are Lamé constants. It is noteworthy that the phase velocity of Rayleigh wave along a curved surface is dependent on the wave frequency and curvature radii besides the elastic constants and density of the material. It can be inferred that suitable frequencies of surface wave are supposed to be applied for different measurement scales.

3 Model development

The following simulation was implemented based on the COMSOL Multiphysics V5.3a. The solid mechanics module was employed for the Rayleigh surface wave studies.

3.1 Geometry & material

The FEM simulation was conducted for existing products of PBXs of specific sizes. The computational model as regards cylindrical surface was established by a two-dimensional geometry. The left side of the geometry was reserved for study of the surface wave propagation along cylindrical surface, and a crack perpendicular to the surface was set on the right side (45° direction). The width of the crack is constantly set to 0.1 mm.

According to the specific material properties provided by the Institute of Chemical Materials (China Academy of Engineering Physics), the approximately isotropic homogeneous material is defined as follows: the density is 1860 kg·m^{-3}, the Young's modulus is 10 GPa and the Poisson's ratio is 0.32. Note that certain PBXs are made of a high-volume

fraction of explosive particles and a very low-volume fraction of binder, especially for the HMX (e.g. PBX 9501) type of PBX that comprises a 95% explosive particle and only 5% binder[14]. It has been proved that the explosive particles are linear elastic at or below room temperature[15]. In addition, the monoclinic crystals (explosive particles) are randomly oriented in PBX[15], so the isotropic elastic properties can be approximately used for this study.

For the spherical surface, a two-dimensional axisymmetric model was built with the same material properties and similar geometry (a crack set on the 45° direction). Fig. 1 shows the schematics of the above configurations. It should be noted that the crack drawn in the figure has been enlarged for clarity. The space around the crack is filled with air.

3.2 Structural mechanics & mesh

The ultrasonic point source was determined by prescribed displacement. A sequence of domain point probes was set on the surface of the geometric model as shown in Fig.1 to receive the ultrasonic signals with respect to the normal and tangential displacement components. Given that surface waves are constrained to a certain depth, two meshes of different densities are deployed to the whole domain. The mesh size of the outer surface layer is $\lambda \cdot 10^{-1}$ where λ is the wavelength, and a predefined extremely fine mesh is set up for the rest. The surface layer is twice as thick as the crack. In order to reduce the wave interference and facilitate the analysis of the signal, a low reflection boundary was determined for the inner surface of the models.

Since the Rayleigh surface waves are excited by point sources determined on the outer faces of the models by prescribed displacements (Hanning windowed sin signals of multi-cycles, the maximum amplitudes are 1×10^{-7} m) towards the normal direction of the surfaces, ultrasonic waves propagating along nearly half space direction are introduced into the models. Except for the expected Rayleigh surface waves which propagate along the outer surfaces, the other inconsequential waves can be diminished to a great extent by the absorption of the low reflection boundary conditions. Note that this excitation method is in certain degree an imitation of laser ultrasonic excitation, which has been used by a few researchers with reasonable results[16-18]. In addition, the ultrasonic near-field effect, which is not pertinent to the scope of this study, is diminutive enough to be neglected according to this particular mechanic load.

3.3 Solver configurations

The numerical simulation involves ultrasonic input signals of 0.25, 0.5, 1.0, 1.5 MHz and 2.0 MHz. The time steps of the transient solver are set as $0.1/f$, where f denotes the frequencies of the excited Rayleigh waves. The above configurations can ensure moderate accuracy of solutions to the specified problems.

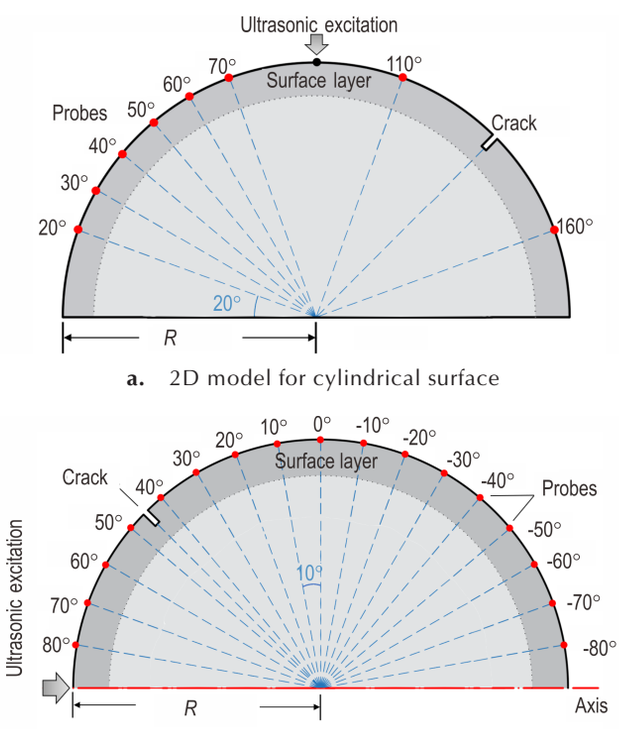

a. 2D model for cylindrical surface

b. 2D axisymmetric model for spherical surface

Fig.1 Geometric models and physical setups

4 Results & discussion

4.1 In cylindrical surface

According to the model developments, an input signal at 1 MHz was brought into the model from

the above of the geometry. The prescribed displacement vertically downward causes surface waves to be generated on the top of the geometry and propagated towards left and right. Firstly, signals picked up by probes on the left side are presented in Fig.2a. As one can see, the normal component of the particle displacement in the cylindrical surface decreases firstly to a certain degree, then rises symmetrically to almost the same values it has reached before. The minimum of the normal displacement is presumed to occur at the 45° position on the left side. In the meanwhile, the trends of decrease and increase are most likely to follow a linear pattern. The tangential displacements seem to be identical as shown in Fig.2b. The above phenomenon can be attributed to the curve of the Rayleigh surface wave guide. For the cylindrical surface, the radii of curvature of the outer surface is R for direction parallel to the figure, and infinite for direction perpendicular to the figure. The wave velocity of Rayleigh surface wave at 1 MHz propagating in cylindrical surface of PBX is calculated as 1302.5 $m \cdot s^{-1}$.

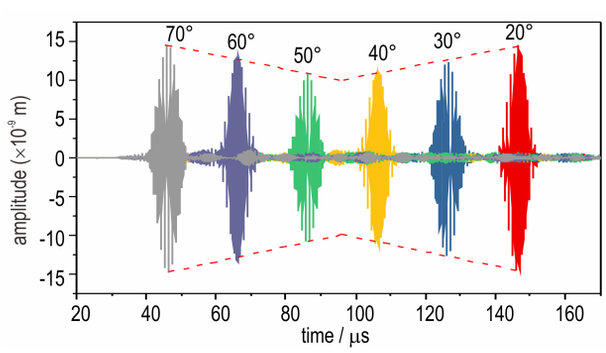

a. normal displacements

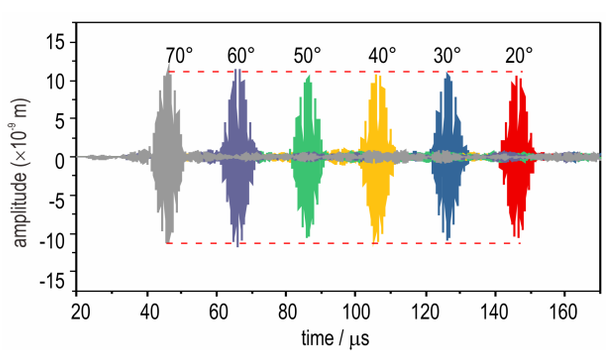

b. tangential displacements

Fig.2 Rayleigh surface waves (1 MHz) received on the cylindrical surface at different positions

For signals collected on the right side of the surface, the Rayleigh surface wave was monitored at the 110° and the 160° positions. The rectangle crack of which the depth is 0.5 mm located at the 45° position was set for the study of crack depth estimation in the PBX. First, we introduce an ultrasonic signal at the frequency of 1 MHz (wavelength 1.3 mm) into the model, and take snapshots of the von Mises surface stress plot of the model. Fig.3 shows the surface wave propagation at different times (0.9×10^{-4}, 1.0×10^{-4}, 1.1×10^{-4} s and 1.5×10^{-4} s). As one can see from Fig.3c, the back scattered waves appear to be greater than the forward scattered waves, since the crack length is as expected long enough ($d/\lambda > 0.3$) to impede the surface wave propagation referring to published experimental results conducted in plate relating to crack depth detection using surface wave[11], and the reflected and transmitted waves propagating along the right side of the surface are monitored by the domain point probes set at the 110° and the 160° positions.

The wavelength of the input ultrasonic signal at the frequency of 1 MHz is about 1.3 mm, and the crack depth ranging from 0.1 mm to 1.1 mm was determined to achieve the above numerical simulations. The ultrasonic surface wave propagated along the curved cylindrical surface and interacted with the surface crack, resulting in the reflected and transmitted waves which were received at the fixed positions (110° and 160°) for the investigation of assess-

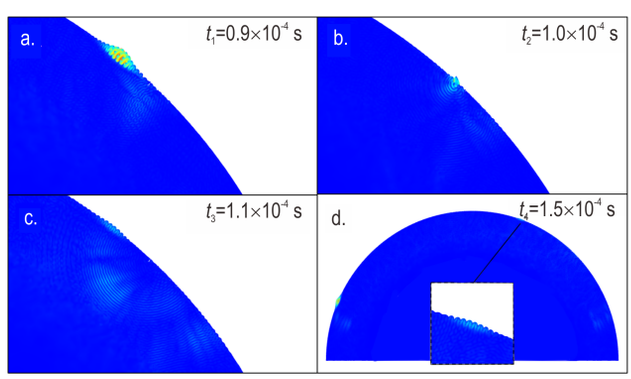

Fig.3 Snapshots of Rayleigh surface waves (1 MHz) on the cylindrical surface at different times

ment of crack depth. Fig.4 shows the maximum amplitudes of the reflected waves and transmission waves with respect to different crack depth. As seen, the maximum amplitudes of the reflected waves increase with the crack depth within certain range (d≤0.4 mm). In a similar way, the maximum amplitudes of the transmission waves decrease with the crack depth within d≤0.4 mm. Therefore, the depth of a crack can be evaluated by measuring the maximum amplitudes of the reflected and transmission waves and concurrently referring to a pre-measured baseline of the relation curves. Note that the maximum amplitude of the reflected waves decreases when the crack depth increases above 0.6 mm, this can be due to the energy scattering of multi wave packets generated from the interaction with the crack.

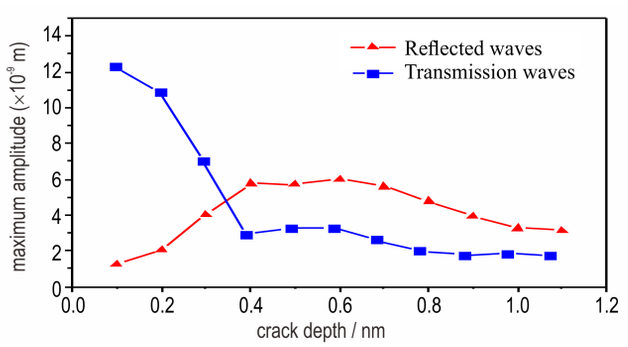

Fig.4 Relation between the maximum amplitudes of reflected and transmission waves and the crack depth (input signal at 1 MHz)

4.2 In spherical surface

4.2.1 Signal analysis

Regarding the spherical surface, similar FEM simulations are achieved adopting the 2D axisymmetric model presented in Fig. 1b, which can be used to enhance the calculation efficiency of the simulation (i.e. by reducing a 3D problem to 2D axisymmetric one). This setup is believed to be reasonable with regard to serval published works[19-20] and the COMSOL Users Guide. First, an ultrasonic signal was introduced into the model in the absence of the crack for study of the wave propagation. As shown in Fig.5, both the normal and tangential components of the particle displacement are altering while the wave propagates along the surface. Especially, the normal displacement of the wave in the spherical surface decays and rises over an approximate exponential trend, while the tangential displacement varies over an approximate linear trend. The minimums of the displacement components are both observed at the 0° position. The curvature of the spherical surface mainly accounts for the above amplitude changes. In addition to the excitation and reception of a signal at the frequency of 0.25 MHz as shown in Fig.5, signal at other frequencies (0.5, 1, 1.5 MHz, and 2 MHz) were also introduced into the model for comparison. An interesting fact is that the amplitude of the Rayleigh surface wave increased back to larger values after propagating through the equator of the model (0° position) when the frequency of the input signal is 0.25 MHz and 0.5 MHz, while the amplitude of the surface wave increased much less after that when the frequency is above 1 MHz. Especially, the amplitude of the surface wave at the frequency of 2 MHz increased a few while propagated to the −80° position

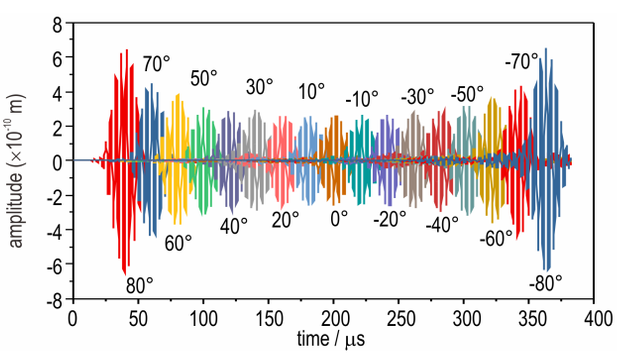

a. normal displacements

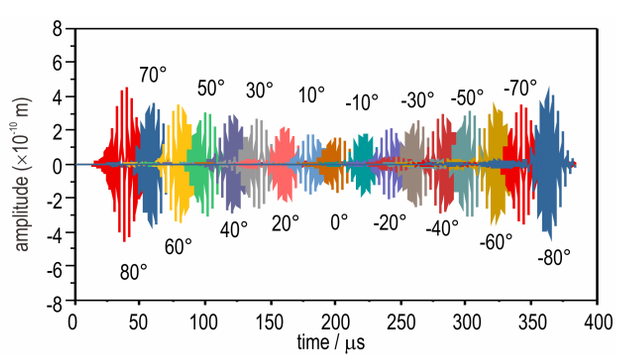

b. tangential displacements

Fig.5 Rayleigh surface waves (0.25 MHz) received on the spherical surface at different positions

compared to that at the 0° position. Besides, the number of cycles of the time domain signal observed from the 0° to −80° positions increased. This phenomenon, which is not presented in figure here, can be attributed to the geometric dispersion of high-frequency ultrasonic signals, embodying the law of conservation of energy.

4.2.2 Motion pattern

To detailly analyze the impact on the amplitude of Rayleigh surface wave by geometrical dispersion in the spherical model, a brief mathematical reasoning is provided here. According to the law of conservation of energy, the total wave energy disperses while the surface wave generated at the displacement point source spreads around the sphere. As shown in Fig. 6a which is in a different perspective from Fig. 1b, the horizontal component of the surface wave velocity satisfies $v_x = v\sin\theta$, the radius of the wave circle thus conforms to $r = \int v_x \,\mathrm{d}\, t = v\cos\theta$. Then the perimeter of the wave circle is $c = 2\pi r = 2\pi v\cos\theta$. Take the total energy of the surface wave as E, the energy of the signal received by the point probe is $e = \frac{E}{c} = \frac{E}{2\pi v}\sec\theta$. As a result, the normal and tangential components of the surface wave detected are processed to represent the total wave energy $E = E_N + E_T = k(d_N^2 + d_T^2)$, where d_N and d_T are the normal and tangential amplitudes of the received signal respectively, and k denotes the conversion coefficient. A mathematic model $E = \frac{E_0}{2\pi v}\cdot\frac{1}{\cos\left(\theta+\theta_0\right)} + e_0$ is then applied to fit the curves of wave energies calculated at different positions. Plots are presented in Fig. 6b, which show decent agreements with the above derivation. It is noted that the energy of signal at the frequency of 0.25 MHz is the largest one among others, which can be due to the identical settings apart from the frequency in the simulations such as the number of excitation cycles and the prescribed amplitudes at the ultrasonic point source.

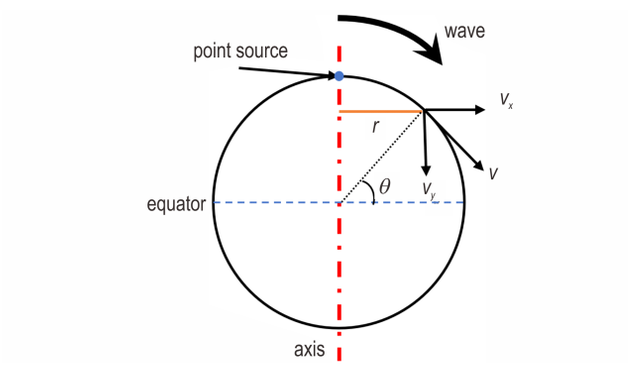

a. schematic of the mathematic reasoning model

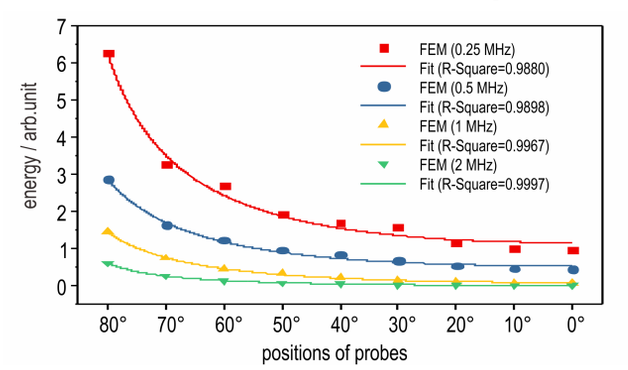

b. energy of the surface waves received at different positions

Fig. 6 Analysis of geometrical dispersion impact on the amplitude of Rayleigh surface wave

In order to understand the motion of particles in more detail, on the other hand, the amplitude ratios of the received surface waves in the normal and tangential directions at different positions are calculated. As shown in Fig. 7a, the amplitude ratio (normal component to tangential component) of the Rayleigh surface wave decreased from the wave source to 45° position, and increased to 1.6 at the equator of the model (0° position). It is interesting to find that the trends of the four different input signals are consistent in terms of the amplitude ratio. In addition, the amplitude ratio reached 1.0 when the surface wave propagated to the 45° position, which suggests that the orbit of the surface particle there is a standard circle. More specifically and vividly, Fig. 7b demonstrated the elliptical orbits of particle motion at different positions. It is noted that the range of motion of the surface particle reduces since the Rayleigh wave disperses from the excitation point source.

The skin effect of the Rayleigh surface wave in the spherical surface is also verified by setting a series of domain point probes at the 45° position under the surface of the model with different depths. As

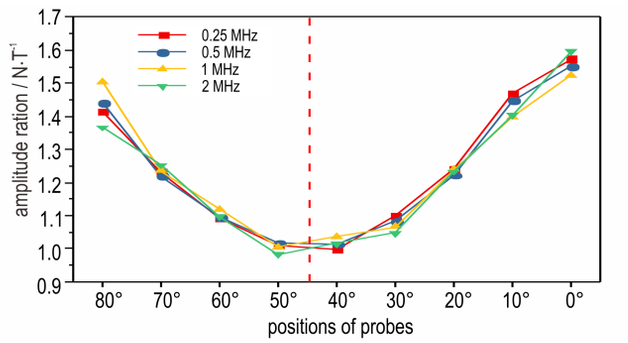

a. the normal amplitude to tangential amplitude ratio

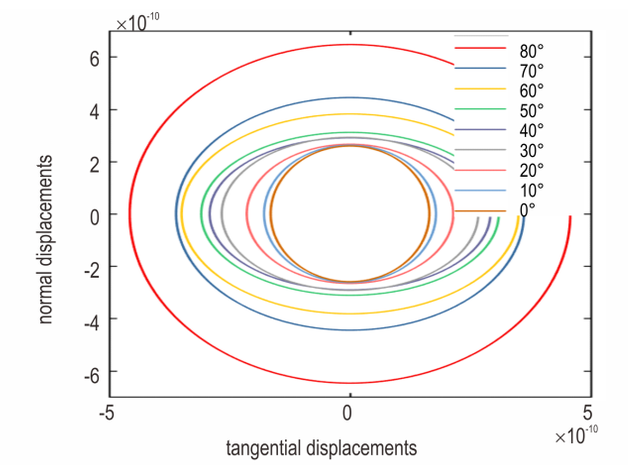

b. the elliptical orbits of the particle motion

Fig.7 Motional pattern of the surface waves

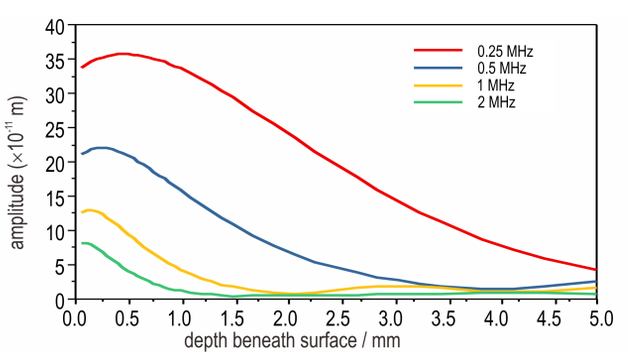

Fig.8 Skin effect of the Rayleigh surface waves at different frequencies

presented in Fig.8, the normal amplitudes of the ultrasonic signals at different frequencies decreases along the depth beneath the surface of the model. Especially, the higher the frequency of the input signal, the smaller the area Rayleigh surface wave can influence. As one can see, the amplitude of the received signal detected 1 mm beneath the surface is rather smaller for input signal at the frequency of 1.5 MHz than others. This fact provides guidance for the frequency selection in the estimation of surface crack depth in the subsequent simulations and future experiments. In addition, the result is in accordance with theory relating to surface wave that the primary wave field is within a wavelength long beneath the surface[13].

4.2.3 Crack depth inversion

Based on the above analyses and the goal to assess the crack depth in PBXs, ultrasonic signals at frequencies of 0.25, 0.5, 1, 1.5 MHz and 2 MHz are brought into the model shown in Fig.1b to investigate the wave reflections and transmissions, respectively. The surface wave detected at the 80°, 70° and 60° are extracted for the analysis of the wave reflections, and signals received at the 30°, 20° and 10° are processed for study of the wave transmissions. As shown in Fig.9, the normal amplitudes of the reflected and transmitted waves at different frequencies vary with the crack depth. Note that the abscissa is labeled as d/λ since the FEM results suggest the wave reflections share almost the same pattern except for slight discrepancies as the frequency of the input signal varies, as well as the wave transmissions. As seen from Fig.9a, amplitudes of signals received near the ultrasonic source (80° for instance) are larger than that away from the source (60° for instance), which suggests that one can set the receiving probes befittingly away from the equator of the future specimen for higher signal-to-noise ratio. Besides, the relation of approximately monotonic decreasing variation between the amplitude of the transmitted wave and the crack depth shown in Fig.9b seems to provide a more feasible and practical way to estimate the crack depth in the spherical surface than the reflected waves. The amplitudes of the reflected and transmitted waves remain almost the same (call it a saturation) when the crack depth reaches to a certain degree, and the local irregularities shown in Fig.9a may be attributed to the interferences of the back scattered waves. As for the tangential components of the reflected waves, Fig.10 shows a similar relationship to Fig. 9a. From a practical

point of view, however, the normal displacement is most likely to be measured in experiments other than the tangential one, even though the tangential component possesses a less variation of amplitude while propagating along the curved surface.

For sufficient accuracy of FEM results ranging from 0 to about 0.3d/λ (d denotes the crack depth), more simulations have been conducted as shown in Fig.11. The frequency of the input signal was determined as 0.25 MHz (wavelength 12 mm). As one can see, due to the relative monotonic variation trend (d/λ <0.23, Fig. 11b). The relation between the crack depth and the normal amplitude of the transmitted wave can be utilized for crack depth estimation. In addition, the reflected waves can also be referred to for reliability considerations. These wave reflection and transmission curves indicate that one can measure a series of benchmarks as references for depth estimation of unknown cracks in the curved surface, and different frequencies can be used for characterization at different length scales. Thus, the inversion method for the crack depth estimation in curved surfaces of this PBX can be described as follows:

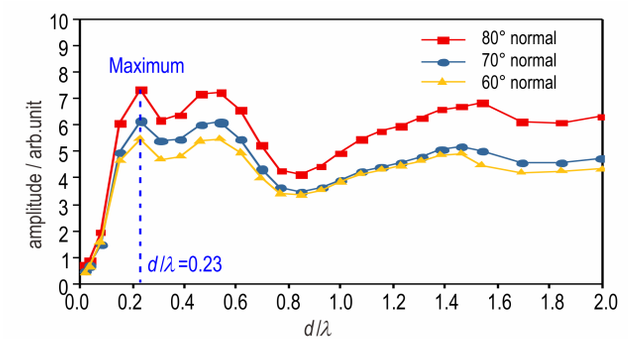

a. reflected waves

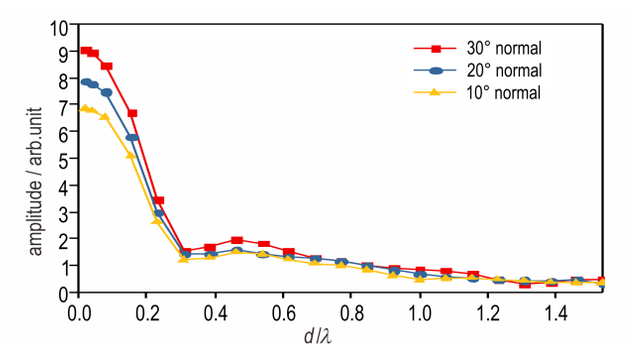

b. transmitted waves

Fig.9 Relation between the crack depth and the normal amplitudes of the waves received at different positions. d, λ denote the crack depth and wavelength of the excited surface wave, respectively

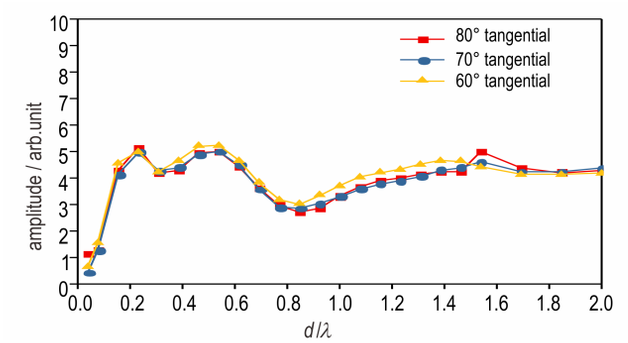

Fig.10 Relation between the crack depth and the tangential amplitudes of the reflected waves at different positions. d, λ denote the crack depth and wavelength of the excited surface wave, respectively

Step 1: For a PBX with unknown depth of crack, introduce a relatively very low-frequency ultrasonic Rayleigh surface wave into the material (e. g. 0.1 MHz for a crack of which depth is below 1mm

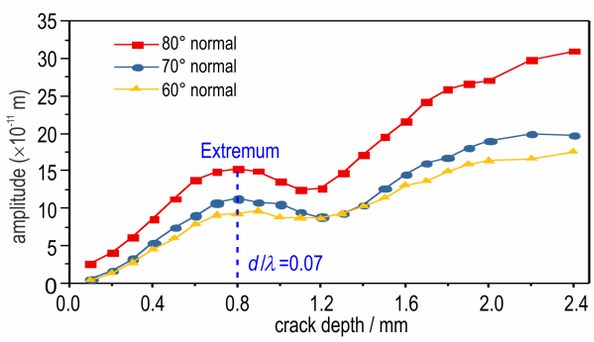

a. reflected waves

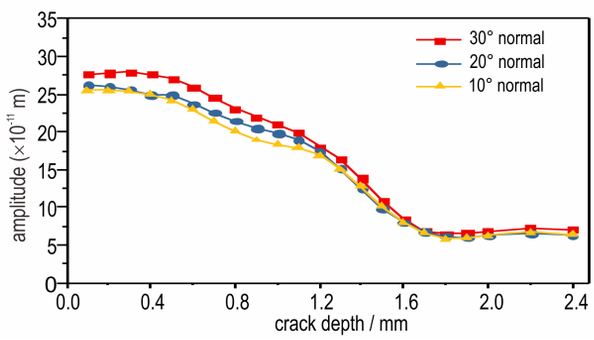

b. transmitted waves

Fig.11 Relation between the crack depth and the normal amplitudes of the waves received at different positions. The frequency of the input signal is 0.25 MHz (wavelength 12 mm)

to ensure d/λ <0.04). In other words, the detection starts from using a long wavelength surface wave to observe the reflected and transmitted waves.

Step 2: By frequency tuning (increase the frequency of the input signal), the wavelength decreases, and the amplitude of transmitted wave drops, along with the increase of amplitude of the reflected wave.

Step 3: When the amplitude of the reflected wave reaches its first extremum (e.g. a local maximum as shown in Fig.11a), continue the frequency increasing with attention.

Step 4: When the amplitude of the reflected wave reaches its first maximum as shown in Fig.9a, the crack depth can be estimated as 0.23λ. Noted that this can be confirmed by repeated implementation of a large range of frequency, as well as the reference of amplitude of the transmitted wave.

It is important to note that the above simulations have not taken the material attenuation into consideration for investigation of surface acoustic waves influenced by geometry and material separately. However, the material attenuation could be determined as constant when the propagation path and properties of the surface wave remain consistent for experimental measurements. Besides, the results are in certain way similar to a published work which was conducted in a cracked plate by electromagnetic acoustic transducer[15]. Thus, the proposed crack estimation method can potentially be promising with credit.

5 Conclusions

(1) The surface wave propagations in cylindrical and spherical surfaces of PBXs are investigated. The general disperse patterns of Rayleigh surface wave motion along these curved surfaces are presented and analyzed.

(2) The wave reflections and transmissions with a single crack by introducing ultrasonic signals at different frequencies are recorded and processed for study of the influences on surface waves by the induced rectangle cracks with various depths.

(3) The numerical simulations indicated that the proposed crack depth estimation method involving transmission waves and reflected waves is potentially viable tools to quantitatively estimate the depth of cracks in the curved surface of PBXs.

(4) Future related experiments are of great significance to achieve the crack location and depth measurement in curved surfaces with the method and results provided in this paper.

References:

[1] Liu J, Liu S, Huang M, et al. Progress on crystal damage in pressed polymer bonded explosives[J]. *Chinese Journal of Energetic Materials*(*Hanneng Cailiao*), 2013, 21(3): 372-378.

[2] Zhang W, Li J, Yang X, et al. Initial mesoscopic damage of TATB based PBX pressed by warm compaction[J]. *Chinese Journal of Energetic Materials*(*Hanneng Cailiao*), 2015, 23(2):202-204.

[3] Yang Z, Tian Y, Zhou H, et al. Detection of micro-damages in TATB-based polymer bonded explosive by nonlinear ultrasonic technique[J]. *Chinese Journal of Energetic Materials* (*Hanneng Cailiao*), 2017, 25(12):970-975.

[4] Yang Z, Tian Y, Li W, et al. Experimental investigation of the acoustic nonlinear behavior in granular polymer bonded explosives with progressive fatigue damage[J]. *Materials*, 2017, 10: 660.

[5] Zong H, Zhang W, Xiao L, et al. Crack depth detection of PBX section by ultrasonic edge peak echo method[J]. *Chinese Journal of Energetic Materials*(*Hanneng Cailiao*), 2016, 24(2):166-170.

[6] Chiffre L D, Carmignato S, Kruth J P, et al. Industrial applications of computed tomography, CIRP Annals[J]. *Manufacturing Technology*, 2014, 63(2):655-677.

[7] Xu P, Chen Z, Chen H, et al. Damage evolution behavior of PBX substitute material using in-situ CT[J]. *Chinese Journal of Energetic Materials* (*Hanneng Cailiao*), 2018, 26(10): 888-895.

[8] Felice M V, Fan Z, Sizing of flaws using ultrasonic bulk wave testing: A review[J]. *Ultrasonics*, 2018, 88:26.

[9] Hassan W, Veronesi W. Finite element analysis of Rayleigh wave interaction with finite-size, surface-breaking cracks[J]. *Ultrasonics*, 2004, 41(1):41-52.

[10] Masserey B, Mazza E. Ultrasonic sizing of short surface cracks [J]. *Ultrasonics*, 2007, 46(3):195-204.

[11] He C, Deng P, Lu Y, et al. Estimation of surface crack depth using Rayleigh waves by electromagnetic acoustic transducers [J]. *Journal of Acoustical Vibration*, 2017, 22(4): 541-548.

[12] Na J K, Blackshire J L. Interaction of Rayleigh surface waves with a tightly closed fatigue crack[J]. *NDT&E International*, 2010, 43(5): 432-439.

[13] Biriukov S V. Surface acoustic waves in inhomogeneous media [M]. Springer, 1995.

[14] Skidmore C, Phillips D, Son S, et al. Characterization of HMX particles in PBX 9501[C]//AIP Conference Proceedings, 1998: 579-582.

[15] Banerjee B, Adams D. On predicting the effective elastic properties of polymer bonded explosives using the recursive cell method[J]. *International Journal of Solids & Structures*, 2004, 41(2):481-509.
[16] Zhan Y, Kong C L X, et al. Experiment and numerical simulation for laser ultrasonic measurement of residual stress[J]. *Ultrasonics*, 2016, 73:271-276.
[17] Guan J, Shen Z, Ni X, et al. Numerical simulation of the ultrasonic waves generated by ring-shaped laser illumination patterns[J]. *Optics & Laser Technology*, 2007, 39(6):1281-1287.
[18] Xu B. Numerical simulation of laser-generated ultrasound by the finite element method[J]. *Journal of Applied Physics*, 2004, 95(4):2116.
[19] Dickinson E, Ekstrom H, Fontes E. COMSOL Multiphysics: Finite element software for electrochemical analysis. A mini-review[J]. *Electrochemistry Communications* 2014, 40:71-74.
[20] Bozkurt E, Gungor U. Validation and benchmarking of COMSOL 2D axisymmetric inductively coupled argon plasma model [C]//9th Ankara International Aerospace Conference, 2017.

基于瑞利表面波的曲面PBX表面裂纹深度检测的数值模拟

江 畅[1,2],杨占锋[1],李卫彬[2],张伟斌[1],田 勇[1]
(1.中国工程物理研究院化工材料研究所, 四川 绵阳 621999; 2.厦门大学航空航天学院, 福建 厦门, 361000)

摘 要: 聚合物黏结炸药(PBXs)在生产、运输和储存的阶段可能会出现裂纹等损伤。炸药的表面裂纹对其物理属性和轰爆性能有重要的影响。表面裂纹深度的定量检测对于加工去除其表面裂纹有重要意义。为了研究利用超声表面波对PBX的表面裂纹进行裂纹深度的检测和表征的可行性,采用有限元数值模拟的方式对超声波在曲面PBX中的传播和散射规律进行研究。对不同频率的瑞利表面波在柱面和球面PBX上传播的运动规律、表面波与不同深度裂纹相互作用的反射和透射规律,以及根据表面波与裂纹的相互作用进行裂纹深度反演进行了研究。有限元数值模拟结果表明曲面PBX上的表面裂纹深度可以通过瑞利表面波的反射波和透射波的幅值变化模式进行推导。

关键词: 瑞利表面波;曲面;聚合物黏结炸药;裂纹;模拟
中图分类号: TJ55; O429; O343 **文献标志码:** A **DOI:**10.11943/CJEM2019156
(责编:高 毅)